Energy Reports 6 (2020) 2913–2918

Contents lists available at ScienceDirect

Energy Reports

journal homepage: www.elsevier.com/locate/egyr

Solid coated $Li_4Ti_5O_{12}$ (LTO) using polyaniline (PANI) as anode materials for improving thermal safety for lithium ion battery

Liuye Mo [a], Haitao Zheng [b,*]

[a] National Engineering Research Center for Marine Aquaculture, Zhejiang Ocean University, Zhoushan, 316022, China
[b] Energy Centre, Council for Scientific and Industrial Research (CSIR), PO Box 395, Pretoria 0001, South Africa

ARTICLE INFO

Article history:
Received 1 June 2020
Received in revised form 22 September 2020
Accepted 15 October 2020
Available online xxxx

Keywords:
Polyaniline
$Li_4Ti_5O_{12}$
Coating
Anode
Thermal safety
Lithium ion battery

ABSTRACT

In generally, the thermal behaviour of cathode and electrolyte are the major concerns for the safety of lithium-ion battery, In contrast to rare attention on thermal effects of anode materials. In this work, $Li_4Ti_5O_{12}$/polyaniline (PANI@LTO) composites were synthesized by solid coating method. The SEM/TEM images of the PANI@LTO composites reveal that the PANI nanorods were crashed and wrapped around the LTO particles. FTIR analysis shows the interaction between the NH groups and the surface of the LTO material by mechanical action, which cause changes of oxidation state of PANI in the PANI@LTO composites, compared with the pristine PANI materials. As an anode material for lithium ion battery, the PANI coatings have improved the rate performance of the LTO materials. The specific capacities of the composite at rates of 2C and 5C are 137.8, and 117.2 $mAhg^{-1}$, which are higher than those of the pristine LTO (99.5 and 77.6 $mAhg^{-1}$, respectively) materials. In addition, the PANI@LTO composites show better cycling stability at 2C rates, after 100 cycles maintained 74.3%, compared to 60.4% of the pristine LTO materials. For thermal behaviour, the test was conducted under 60 °C at 2C rate, the initial capacity of the PANI@LTO composites was 152.5 $mAhg^{-1}$ that is higher than the value of 137.8 $mAhg^{-1}$at room temperature. However, the pristine LTO materials show similar initial capacity with that at room temperature. In addition, the PANI@LTO composites maintain better thermal stability, the capacity of the PANI@LTO composites were retained 83.2% after 80 cycles at 60 °C, compared to 54% loss on the LTO electrode under same condition. These results suggest that PANI might be a promising material to improve capacity and benefit thermal safety of lithium ion battery.

1. Introduction

Over the decades, spinel-type $Li_4Ti_5O_{12}$ (LTO) has been explored as a promising alternative anode material, especially in large-scale batteries, such as hybrid electric vehicles (HEVs) or renewable energy storage plants, as a result of its important properties including low cost, abundance, and environmental friendliness. However, there are safety considered problems in the larger batteries that caused from shorting or increased external temperature. On the whole, the thermal behaviour of cathode and electrolyte are considered to interfere safety of lithium ion battery. And the thermal stability of anode materials is rarely paid attentions (Wen et al., 2016; Liu et al., 2018). The LTO material is a kind of zero strain material with a negligible volume change during intercalation/deintercalation process (Yi et al., 2020b; Wang et al., 2019b). It has relatively high operating voltage plateau (1.55 V vs. Li/Li^+), which minimizes the electrolyte decomposition and forms a solid electrolyte interphase (SEI). These properties of the LTO materials contribute to a long cycling life of the LIBs, which allowing the LIBs to withstand the rapid charge/discharge cycle required for many modern applications. However, one practical issue associated with the LTO is its low theoretical capacity (175 mAh g^{-1}) and poor capacity at high rate, which mainly resulted from its inherent low electronic conductivity and poor Li^+ diffusion coefficient. In order to solve this problem, some approaches were explored through coating with carbon materials, conducting polymers and doping with other elements etc. (Yi et al., 2020b; Roh et al., 2020; Uceda et al., 2020; Medina et al., 2015; Ncube et al., 2018).

Since Shirakawa et al. discovered polyacetylene can be oxidized/reduced for the first time in 1977 (Shirakawa et al., 1977). Various polymers have been proposed for charge storage, and the key parameters of polymer batteries were also critically discussed (Shi et al., 2015; Novák et al., 1997). In practical terms, it is revealed that low density and low charge density per surface area of polymer battery arouse serious problems where energy density and electrode areas are concerned (Passiniemi and Österholm, 1987). To address the issues, the polymer composites as electrode materials have been studied intensively (Shi et al., 2015; Ćirić-Marjanović, 2013), in particular, polyaniline as active matrices to

* Corresponding author.
E-mail address: hzheng@csir.co.za (H. Zheng).

https://doi.org/10.1016/j.egyr.2020.10.018

improve the capacity, cycling stability and rate performance of anode for LIBs (Wang et al., 2016a; Hui et al., 2017; Chen et al., 2012; Ma et al., 2015; Wang et al., 2014; Yi et al., 2019; Zheng et al., 2016). On one hand, the polymer can serve as a conducting backbone for the active materials. On the other hand, during intercalation/deintercalate of Li, the internal stresses/strains and the structural integrity of the polymeric composite can be accommodated through the inert matrix (Yi et al., 2019; Zheng et al., 2016; Yi et al., 2020a; Karthikeyan et al., 2013). From literature reports (Yi et al., 2020b; Wang et al., 2016a; Hui et al., 2017), the synthesis methods for the polyaniline composites were mainly focused on in-site approach. In this work, we use simple solid coating to modify LTO in order to improve conductivity of the LTO, so as to achieve better capacity.

2. Experiential

2.1. Synthesis of polyaniline (PANI)

Polyaniline was synthesized by chemical polymerization. Aniline monomer (3.75 g) was dissolved in 100 ml of 0.02M HCl aqueous solution and stirred for 30 min at 0–5 °C. Then $(NH_4)_2S_2O8$ (7.2 g) was added to the above solution. The mixture was kept overnight at 0–5 °C. The precipitate was washed with deionized water and methanol, separately, and then finally dried overnight in a vacuum at 70 °C.

2.2. Synthesis of $Li_4Ti_5O_{12}$ and $Li_4Ti_5O_{12}$/PANI composites

$Li_4Ti_5O_{12}$ was synthesized by a solid-state reaction method described in literature (Wen et al., 2015) using Anatase TiO_2 (∼220 nm, 99.5%, Hangzhou Wanjing New Material Co., Ltd) and Li_2CO_3 (99.9%, Shanghai China Lithium Industrial Co., Ltd.) as raw materials. The Li_2CO_3 and TiO_2 were mixed using ball-milling with molar ratio of Li: Ti = 0.82:1. The mixture then was calcined at 800 °C in air for 18 h, followed by grinding to obtain the final $Li_4Ti_5O_{12}$ product.

The as-synthesized LTO and PANI were mixed by ball milling to form PANI@LTO composites with 5% wt. of PANI.

2.3. Characterization

The morphologies and structures of PANI@LTO, LTO and PANI were characterized by a using X-ray diffraction (XRD, SCINTAG-XDS 2000), a Hitachi H-7000 transmission electron microscope (TEM, JOEL2010, 200 kV), and a scanning electron microscopy coupled to energy dispersive spectroscopy (SEM/EDS) measurements (JSM-7500F SEM/EDS).

2.4. Coin cell assembly and electrochemical measurements

Procedure of coin cells assembling was as followed. The synthesized composites PANI@LTO or LTO were mixed with carbon black (PRINTEX XE 2-B) and PVDF with ratio of 80:10:10 wt% to fabricate anode ink. In the coin-cell (CR2032) test, metallic lithium foil was used as the counter and reference electrodes; the electrolyte was 1 mol/L $LiPF_6$ in a 1:1 mixture of ethylene carbonate and diethyl carbonate (EC/DEC). Electrochemical measurements were carried out between 1.0 and 2.5 V vs. Li^+/Li^0. Capacity of the cell was calculated on the basis of the total mass of the active material. The mass of the active materials in coin cell was 5 ± 0.2 mg.

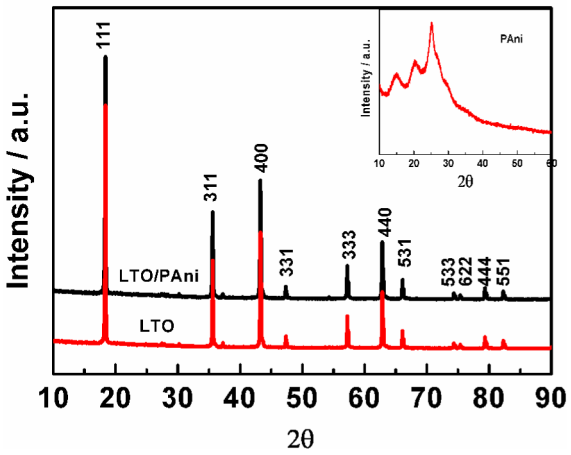

Fig. 1. XRD pattern of LTO, PANI (inset) and PANI@LTO materials.

3. Results and discussion

The XRD patterns of the PANI, PANI@LTO and LTO materials are showed in Fig. 1. The XRD patterns of the PANI revealed the typical diffraction peaks of polyaniline at 14.9°, 20.4° and 25.0°, respectively, as displayed inset of Fig. 1. It can be seen from Fig. 1, all diffraction peaks of the LTO materials are match to the cubic spinel structure without impurities (PDF card No.49–0207). The same diffraction peaks of the LTO were appeared in the PANI@LTO materials without the PANI peaks, compared with patterns of LTO materials. This might be related to lower PANI amount in PANI@LTO that lead to diffraction peaks of PANI merged with the peak [111] of the LTO located in similar position.

3.1. Morphology

Fig. 2 shows the SEM/TEM morphology of the PANI, LTO and PANI@LTO materials. It can be seen from Fig. 2a image, PANI are nanorods with around 45 nm diameter and 200–300 nm in length. Fig. 2b displays LTO particles are in the size range from 0.1 to 1.2 μm. After milling LTO with PANI, the PANI nanorods were disappeared in SEM image as given in Fig. 2c, which are probably because the PANI nanorods were crashed and covered on the LTO particles. For further identify the morphology of the PANI@LTO, TEM image of the PANI@LTO was shown in Fig. 2d. The PANI layer can be observed distinctly in Fig. 2d, which indicates the PANI was coated on the LTO particles.

The FTIR spectra of the PANI and the PANI@LTO materials are shown in Fig. 3. The typical peaks of the PANI was displayed in Fig. 3 at 1511.2 and 1623.2 cm^{-1}, corresponding to the functional C=C stretching vibrations of benzenoid and quinoid rings (Jain et al., 2016), respectively. The absorption peaks of the PANI spectra at 829.8, 1191.0, 1315.2, 1352.0 cm^{-1}, which agree with C-H bonding from aromatic rings, N=Q=N stretching vibrations of quinoid (Q), C-N stretching and C=N vibration from iminoquinon (Quillard et al., 1994). For the PANI@LTO sample, the big broad peak between 476–1010 cm^{-1} can be ascribed to the symmetric and asymmetric stretching vibrations of the TiO6 octahedron of LTO (Zhao et al., 2016). Compared to the PANI spectrum, the peaks of the PANI@LTO spectrum in range of 1250–2500 cm^{-1} from Fig. 3 were red shifted slightly with lower densities of the PANI absorption bands due to its low amount in the PANI@LTO. The shift might be owing to the interaction between the NH groups of PANI and the surface of the LTO particles. Such Interaction was also observed on the PANI composites with other oxides (He, 2005; Liu et al., 2016). For pure PANI, the band intensity

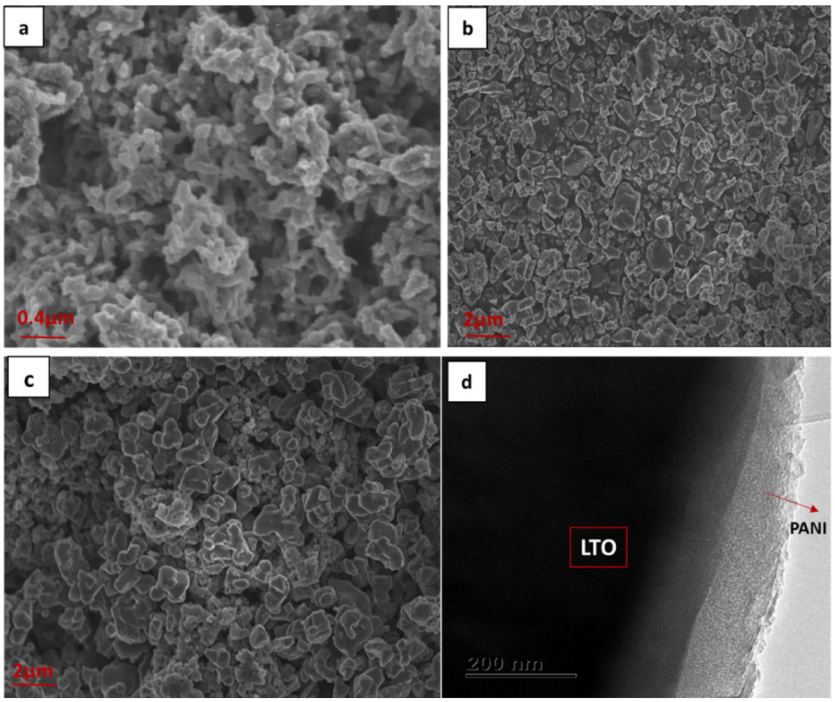

Fig. 2. SEM images of PANI (a), LTO (b), and PANI@LTO (c) and TEM image of PANI@LTO (d).

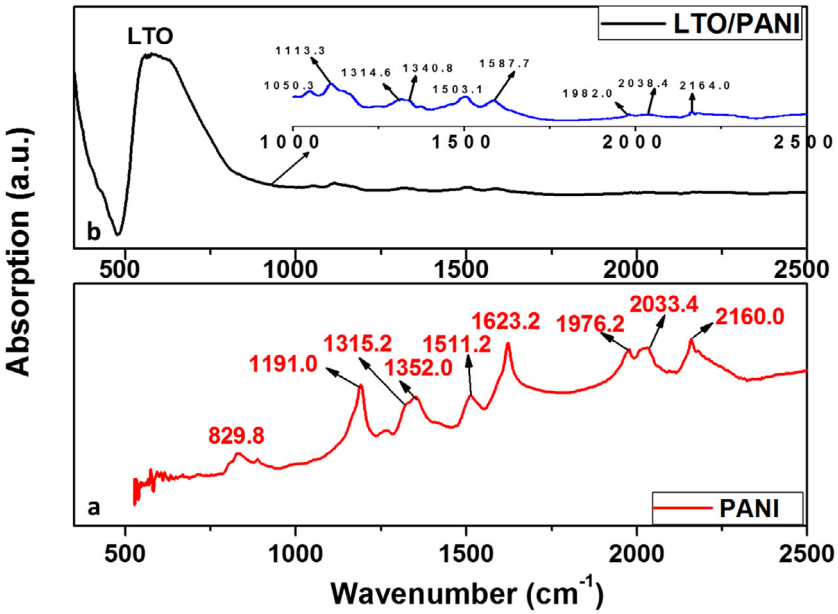

Fig. 3. FTIR spectra of PANI@LTO and PANI materials; the blue line is zoom of PANI@LTO between 1000–2500 cm^{-1}. (For interpretation of the references to colour in this figure legend, the reader is referred to the web version of this article.)

of quinoid rings is much higher than that of the benzenoid ring, which is consistent with the characteristic of PANI (Baibarac et al., 2011). Contrary to the PANI, it is interesting noted the intensity of benzenoid band is slightly higher than that of the quinoid band in the PANI@LTO. This clearly indicates changes of PANI oxidation degree caused from surface interaction between PANI and LTO. Moreover, similar phenomenon was also observed on bands of 1315.2 and 1352.0 cm^{-1} on the PANI@LTO, which further reveals the interaction between the PANI and the LTO.

3.2. Electrochemical performance

The shapes of redox peaks from cyclic voltammograms (CV) curves reflect the electrochemical reaction kinetics of Li^+ insertion/deinsertion. A sharp and well-resolved peak generally signifies fast Li^+ insertion/deinsertion, whereas a broad peak suggests a sluggish process (Shi et al., 2011). The electrochemical performance of the PANI@LTO and the LTO were characterized by CV within a potential window of 1.0 –2.5 V (vs. Li/Li^+) at various scan rates, as shown in Fig. 4. In Fig. 4a, the LTO electrode has displayed single redox peaks at various scan rates, corresponding to Li insertion/extraction. Fig. 4b shows similar redox peaks with

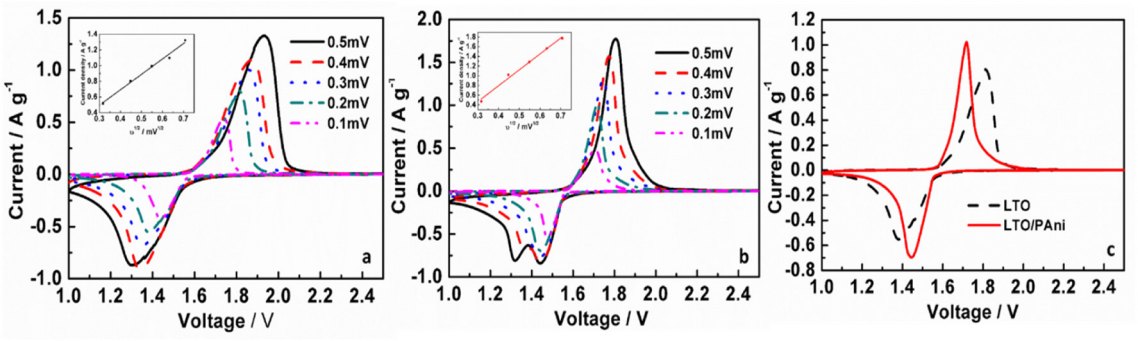

Fig. 4. CV curves at different scan rate and the linear relations of peak current and the square root of the scan rate (inset), LTO (a); PANI@LTO (b); comparison of LTO and LTO/ PANI electrodes at scan rate of 0.1 mV s^{-1}(c).

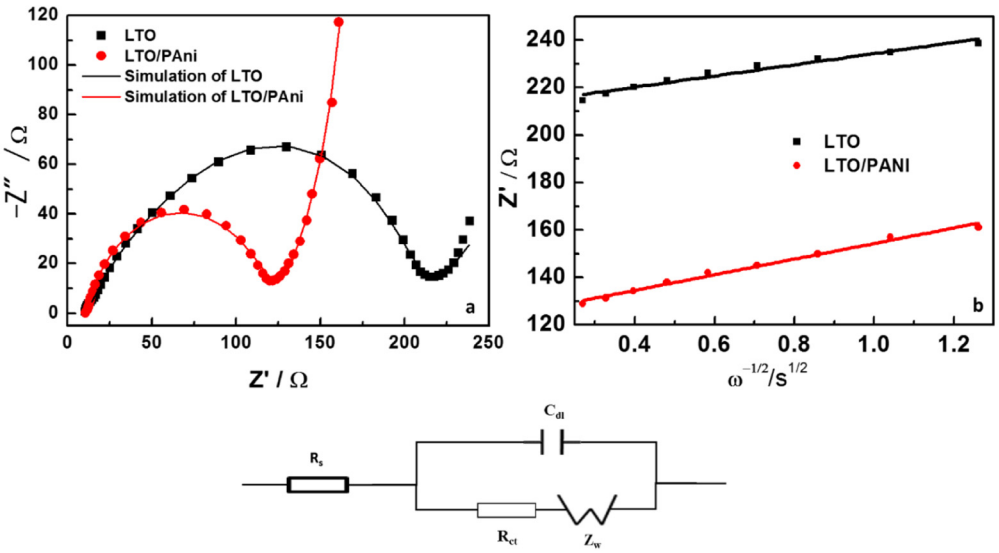

Fig. 5. Electrochemical impedance spectroscopy (EIS) of the LTO/GNRs and the LTO electrode; Equivalent circuit of LTO and PANI@LTO cell. R, C and Z_w refer to charge-transfer resistance, double-layer capacitance and warburge impedance, respectively (inset).

those of the LTO electrode at low scan rates ($\leq$0.3 mV s^{-1}). However, there are two cathodic peaks on the PANI@LTO at higher scan rate, the extra peak can be attributed to the Li^+ doping in the PANI (Wang et al., 2016a). Fig. 4c displays CVs comparison of the two materials, compared to the LTO, on the PANI@LTO electrode, there is sharp redox peaks with narrow distance between redox peaks, indicating increased Li^+ insertion/deinsertion reaction kinetics. Moreover, the onset potential of the PANI@LTO electrode has shifted negatively with higher current density of redox peaks, which shows the PANI@LTO electrode has higher electrochemical activity than that of the LTO electrode. From inset graphs of Fig. 4a and b, we can see that peak current (j) displays a linear relation with the square root of the scan rate ($\nu^{1/2}$), which is considered as a diffusion-controlled progress rather than the surface control on both electrodes. The results have shown that PANI additives have accelerated reaction kinetics without influence on reaction kinetics path.

Electrochemical impedance spectroscopy (EIS) were recorded at 1.55 V from 500 kHz to 100 mHz on fresh coin cells, as shown in Fig. 5. The plot of Z′ vs. the reciprocal root square of the lower angular frequencies (ω) is displayed in Fig. 5b. An equivalent circuit simulated from EIS on both materials are included in Fig. 5. It can be observed from Fig. 5a that the capacitive semicircles on high frequencies were displayed on both electrodes. For lower frequencies, the ~45° slopes on both electrodes were described as the typical Warburg impedances (Z_w) results from a semi-infinite diffusion of Li^+ ion in the electrode (Krewer et al., 2006; Wang et al., 2019a; Tian et al., 2010). In addition, values of simulations were listed on Table 1. It can be seen from Table 1, internal resistance (R_s) of LTO was slightly decreased by coating PANI. The semicircle of PANI@LTO was smaller than that of the LTO, which indicates that the solid-state interface layer and charge transfer resistance (R_{ct}, 109.4 Ω) are lower than that of the LTO (138.3 Ω). The resistance of the solid-state interface layer PANI additive is probably responsible for the increasing of the electronic conductivity of the PANI@LTO. It can be deduced that adding PANI Lead to the formation of thinner interface layer and reduced transfer resistance on the PANI@LTO composites which make transfer rate of Li-ion in the LTO structure dramatically improved (Wang et al., 2016b). On the other hand, the lower charge-transfer resistance of the PANI@LTO cell led to higher exchange current densities based on the formula ($j = RT/nFR_{ct}$) (see Table 1). An exchange current density ($j = 2.34 \times 10^{-4}$ mA cm^2) was obtained on the PANI@LTO electrode, which is higher than that of the LTO electrode ($j = 1.86\times10^{-4}$ mA cm^2). The faster charge-transfer kinetics of the PANI@LTO electrode could be attributed to PANI, which enhanced the conductivity of the electrode. However, The D_{Li} value for the LTO/PANI electrodes is 1.87×10^{-12} cm^2 s^{-1}, which is slightly lower than the value of 1.58×10^{-12} cm^2 s^{-1} of the LTO electrodes. The results indicate that the PANI coatings increased the LTO conductivity and slightly decreased migration of lithium ions.

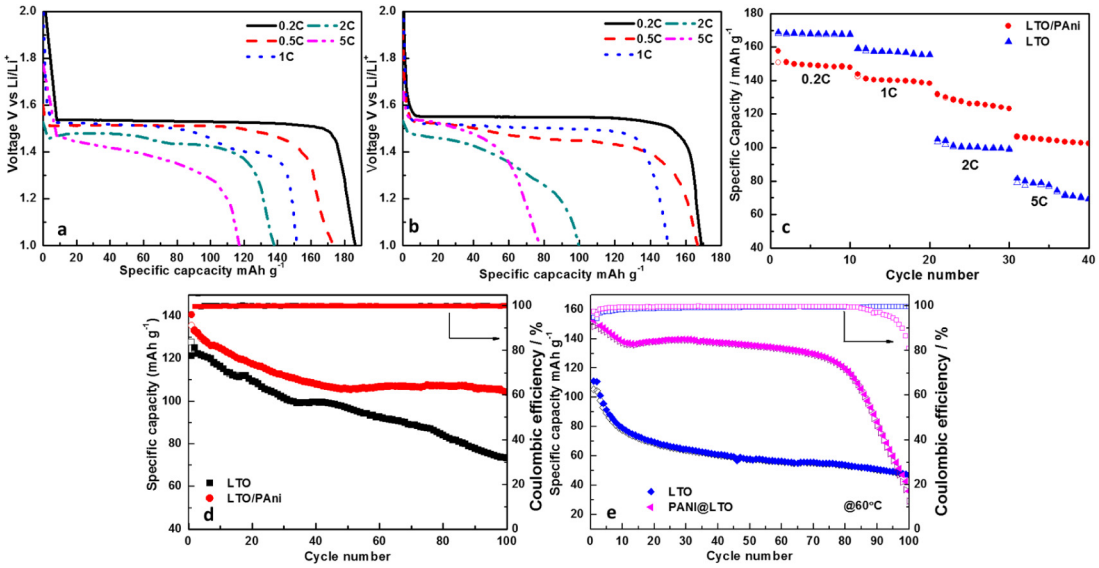

Fig. 6. Initial discharge/charge capacities at different rates on LTO electrode (a); PANI@LTO electrode (b); Rate capability of the PANI@LTO and the LTO electrode at different rates (c); cycling performance and coulombic efficiency on LTO and PANI@LTO electrodes for 100 cycles at room temperature (d) and 60 °C (e) at the rate of 2 C.

Table 1
Electrochemical quantitative analysis from CVs and EIS on the LTO and the PANI@LTO electrodes.

Electrodes	R_s (Ω)	R_{ct} (Ω)	j/mA cm^2	σ_w/Ω cm^2 s$^{-1/2}$	D/cm^2 s^{-1}
LTO	11.9	138.3	1.86×10^{-4}	20.4	1.87×10^{-12}
PANI@LTO	11.2	109.4	2.34×10^{-4}	23.42	1.58×10^{-12}

The Li^+ diffusion coefficient values (D_{Li}) were calculated using Eq. (1) and listed in Table 1.

$$D_{Li} = \frac{1}{2}\left(\frac{RT}{An^2F^2C\sigma}\right)^2 \quad (1)$$

In which, A is active surface area of electrode (1.54 cm^2); R is the gas constant (8.314 J mol^{-1} K^{-1}); T is the testing temperature (298 K); n is the number of electrons transferred (n = 1); F is the Faraday constant (96 485 C mol^{-1}); C is the concentration of Li^+ in LTO solid (4.37×10^{-3} mol cm^{-3}); σ is the Warburg impedance coefficient that can be obtained from the slop of the lines in Eq. (2) (Wang et al., 2019a).

$$Z' = R_s + R_{ct} + \sigma\omega^{-1/2} \quad (2)$$

3.3. Battery performance

The battery performance regarding specific capacity, charge/discharge and cycling ability, of the PANI@LTO composites and the LTO were tested, at various charge/discharge rates from 0.2 C to 5 C in the potential range of 1–2.5 V vs. Li/Li^+, as displayed in Fig. 6. When comparing Fig. 6a and b, both electrodes display flat potential plateaus at low rates (0.2 C – 1 C). However, when increasing the rate, the potential plateaus of the LTO became shorter and gradually bent. This could result from an increase of polarization on pure LTO at higher rate, while that of the PANI@LTO electrode still remains flat at 2 C (Fig. 6b). At low rates of 0.2 C, 0.5 C and 1 C, the specific capacities of PANI@LTO composites were 186.4, 173.4 and 151.7 mAh g^{-1}, respectively. There are slightly lower capacity shown in LTO (169, 166.7 and 149 mAh g^{-1} at 0.2 C, 0.5 C and 1 C, respectively). An ideal battery should provide maximum capacity with same value of the theoretical capacity. In reality, internal losses turn some energy into heat and lower the resulting capacity to less of 100 percent. Discharging the same battery at low 1 C will likely increase the capacity to above 100 percent. That is reason why the capacity of 186.4 mAh g^{-1} at 0.2 C is over theoretical capacity of 175 mAh g^{-1} of LTO on the PANI@LTO. At higher charge/discharge rates of 2 C and 5 C, the specific capacities of PANI@LTO were 137.8 and 117.2 mAh g^{-1}, respectively, which is ∼ 40 mAh g^{-1} greater than those of the pure LTO (99.5 and 77.6 mAh g^{-1}, respectively). This also implies that the PANI@LTO electrode has lower polarization due to the improved electrical conductivity produced by the PANI.

Fig. 6d shows the initial discharge capacities of the LTO and the PANI@LTO were 127.4 and 140.6 mAh g^{-1}, respectively, and the retained discharge capacities were 60.4% and 74.3% mAh g^{-1} after 100 cycles. It is obviously the PANI@LTO has better cycling stability than that of the LTO. The coulombic efficiencies on both electrodes remain around 100% through 100 cycles.

Commercial lithium-ion batteries are thermally stable up to ∼60 °C (Zhang et al., 2002), above which their performance declines. Anode/electrolyte reactions occur first (MacNeil et al., 2002), while cathode/electrolyte reactions dominate the heat-evolution processes at elevated temperatures (Richard and Dahn, 1999). Considering this issue of battery, the LTO and the PANI@LTO anodes were cycled with 2 C rate for 100 cycles at 60 °C. Compared to the values at room temperature, the initial discharge capacity of the LTO was decreased to 111.2 mAh g^{-1} at 60 °C; while in case of the PANI@LTO, its initial discharge capacity was increased to 152.5 mAh g^{-1}. It is worth to note that capacity of the PANI@LTO composites still remain 83.2% (135.7 mAh g^{-1}) after 80 cycles. Only 57.8 mAh g^{-1} left on the LTO electrode with 54% loss. The coulombic efficiency of the PANI@LTO (Fig. 6e) shows slightly higher than that of the LTO up to 80 cycles. At high temperature, battery operation is inhibited as a result of increased internal resistance caused by polymer and ionic liquid phase separation (Kelly et al., 2015). From this point, PANI probably prevents the separation and then lead to less increased internal resistance. On the other hand, high temperature might improve contact surface between LTO and PANI regarding PANI's polymer property. However, after 80 cycles, there is a sharp decline of capacity on the PANI@LTO electrode due to reaction between the PANI and electrolyte/ as well as degradation of the PANI. It can be a solution to the problem by choosing different electrolyte.

4. Conclusion

PANI@LTO composites were prepared through solid coating method. The LTO/ PANI composites have showed improved reversible capacity and cycling stability compared with pure LTO. Especially in higher charge/discharge rates of 2 C and 5 C, the specific capacities of PANI@LTO were 137.8 and 117.2 mAh g^{-1}, respectively, which is $\sim$ 40 mAh g^{-1} greater than those of the pure LTO (99.5 and 77.6 mAh g^{-1}, respectively). The capacity of PANI@LTO composites has retained 83.2% after 60 cycles, and 54% loss on LTO electrode under same condition. The potential impact of PANI coatings is to increase the rate capacity and thermal safety of lithium ion battery.

Declaration of competing interest

The authors declare that they have no known competing financial interests or personal relationships that could have appeared to influence the work reported in this paper.

Acknowledgements

Thanks for Financial supported from Council for Scientific and Industrial Research (CSIR) of South Africa; NSFC-Zhejiang Joint Fund for Integration of Industrialization and Diversification (U1809214) and Zhoushan city science & technology research project (2019C21012).

References

Baibarac, M., Baltog, I., Lefrant, S., 2011. Recent progress in synthesis, vibrational characterization and applications trend of conjugated Polymers/Carbon Nanotubes composites. Curr. Org. Chem. 15, 1160–1196.

Chen, M., Du, C., Wang, L., Yin, G., Shi, P., 2012. Silicon/Graphite/Polyaniline nanocomposite with improved lithium-storage capacity and cyclability as anode materials for Lithium-ion Batteries. Int. J. Electrochem. Sci. 7, 819–829.

Ćirić-Marjanović, G., 2013. Recent advances in polyaniline composites with metals, metalloids and nonmetals. Synth. Met. 170, 31–56.

He, Y., 2005. A novel emulsion route to sub-micrometer polyaniline/nano-ZnO composite fibers. Appl. Surf. Sci. 249, 1–6.

Hui, Y., Cao, L., Xu, Z., Huang, J., Ouyang, H., Li, J., Hu, H., 2017. In situ synthesis of Core-Shell $Li_4Ti_5O_{12}$ @Polyaniline composites with enhanced rate performance for Lithium-ion battery Anodes. J. Mater. Sci. Technol. 33, 231–238.

Jain, R., Sinha, A., Khan, A.L., 2016. Polyaniline-graphene oxide nanocomposite sensor for quantification of Calcium Channel Blocker levamlodipine. Mater. Sci. Eng. C 65, 205–214.

Karthikeyan, K., Amaresh, S., Aravindan, V., Kim, W., Nam, K., Yang, X., Lee, Y., 2013. $Li(Mn_{1/3}Ni_{1/3}Fe_{1/3})O_2$-polyaniline hybrids as cathode active material with ultra-fast charge–discharge capability for lithium batteries. J. Power Sources 232, 240–245.

Kelly, J.C.N., Degrood, L., Roberts, M.E., 2015. Li-ion battery shut-off at high temperature caused by polymer phase separation in responsive electrolytes. Chem. Commun. 51, 5448–5451.

Krewer, U., Christov, M., Vidakovic, T., Sundmacher, K., 2006. Impedance spectroscopic analysis of the electrochemical methanol oxidation kinetics. J. Electroanal. Chem. 589, 148–159.

Liu, P., Li, L., Yao, Z., Zhou, J., Du, M., Yao, T., 2016. Synthesis and excellent microwave absorption property of polyaniline nanorods coated $Li_{0.435}Zn_{0.195}Fe_{2.37}O_4$ nanocomposites. J. Mater. Sci.: Mater. Electron. 27, 7776–7787.

Liu, K., Liu, Y., Lin, D., Pei, A., Cui, Y., 2018. Materials for lithium-ion battery safety. Sci. Adv. 4, eaas9820.

Ma, R., Wang, M., Dam, D.T., Yoon, Y., Chen, Y., Lee, J., 2015. Polyaniline-coated Hollow Fe2O3 nanoellipsoids as an Anode material for high-performance Lithium-Ion batteries. ChemElectroChem. 2, 503–507.

MacNeil, D., Lu, Z., Chen, Z., Dahn, J.R., 2002. A comparison of the electrode/electrolyte reaction at elevated temperatures for various Li-ion battery cathodes. J. Power Sources 108, 8–14.

Medina, P., Zheng, H., Fahlman, B., Annamalai, P., Swartbooi, A., Le Roux, L., Mathe, M., 2015. $Li_4Ti_5O_{12}$/graphene nanoribbons composite as anodes for lithium ion batteries. SpringerPlus 4 (643).

Ncube, N.M., Mhlongo, W.T., McCrindle, R.I., Zheng, H., 2018. The electrochemical effect of Al-doping on $Li_4Ti_5O_{12}$ as anode material for lithium-ion batteries. Mater. Today: Proc. 5, 10592–10601.

Novák, P., Müller, K., Santhanam, K., Haas, O., 1997. Electrochemically Active Polymers for rechargeable Batteries. Chem. Rev. 97, 207–282.

Passiniemi, P., Österholm, J., 1987. Critical aspects of organic polymer batteries. Synth. Met. 18, 637–644.

Quillard, S., Louarn, G., Lefrant, S., MacDiarmid, A., 1994. Vibrational analysis of polyaniline: A comparative study of leucoemeraldine, emeraldine, and pernigraniline bases. Phys. Rev. B. 50, 12496–12508.

Richard, M., Dahn, J., 1999. Accelerating rate calorimetry study on the thermal stability of lithium intercalated graphite in electrolyte. II. Modeling the results and predicting differential scanning Calorimeter curves. J. Electrochem. Soc. 146, 2078–2084.

Roh, H., Lee, G., Haghighat-Shishavan, S., Chung, K., Kim, K., 2020. Polyol-mediated carbon-coated $Li_4Ti_5O_{12}$ nanoparticle/graphene composites with long-term cycling stability for lithium and sodium ion storages. Chem. Eng. 385 (12398).

Shi, Y., Peng, L., Ding, Y., Zhao, Y., Yu, G., 2015. Nanostructured conductive polymers for advanced energy storage. Chem. Soc. Rev. 44, 6684–6696.

Shi, Y., Wen, L., Li, F., Cheng, H., 2011. Nanosized $Li_4Ti_5O_{12}$/graphene hybrid materials with low polarization for high rate lithium ion batteries. J. Power Sources 196, 8610–8617.

Shirakawa, H., Louis, E.J.A., MacDiarmid, G., Chiang, C.K., Heeger, A.J., 1977. Synthesis of electrically conducting organic polymers: halogen derivatives of polyacetylene, (CH)x. J. Chem. Soc. Chem. Commun. 16, 578–580.

Tian, B., Xiang, H., Zhang, L., Li, Z., Wang, H., 2010. Niobium doped lithium titanate as a high rate anode material for Li-ion batteries. Electrochim. Acta 55, 5453–5458.

Uceda, M., Chiu, H., Gauvi, R., Zaghib, K., Demopoulos, G., 2020. Electrophoretically co-deposited $Li_4Ti_5O_{12}$/reduced graphene oxide nanolayered composites for high-performance battery application. Energy Storage Mater. 26, 560–569.

Wang, B., Gu, L., Zhang, D., Wang, W., 2019a. High-throughput production of Zr-Doped $Li_4Ti_5O_{12}$ modified by mesoporous Libaf3 nanoparticles for superior lithium and Potassium Storage. Chem. Asian J. 14, 3181–3187.

Wang, S., Hu, L., Hu, Y., Jiao, S., 2014. Conductive polyaniline capped Fe_2O_3 composite anode for high rate lithium ion batteries. Mater. Chem. Phys. 146, 289–294.

Wang, H., Lin, J., Shen, Z.X., 2016a. Polyaniline (PANi) based electrode materials for energy storage and conversion. J. Sci.: Adv. Mater. Dev. 1, 225–255.

Wang, H., Lin, J., Shen, Z.X., 2016b. Polyaniline (PANi) based electrode materials for energy storage and conversion. J. Sci.: Adv. Mater. Dev. 1, 225–255.

Wang, Q., Mao, B., Stoliarov, S., Sun, J., 2019b. A review of lithium ion battery failure mechanisms and fire prevention strategies. Prog. Engergy Combust. 73, 95–131.

Wen, L., Luo, H., Liu, G., Zheng, H., 2016. Nanomaterials in Advanced Batteries and Supercapacitors. Springer, p. 127.

Wen, L., Wu, Z., Luo, H., Song, R., Li, F., 2015. Dual functions of carbon in $Li_4Ti_5O_{12}$/C Microspheres. J. Electrochem. Soc. 162 (A3038).

Yi, T., Mei, J., Peng, P., Luo, S., 2019. Facile synthesis of polypyrrole-modified Li5Cr7Ti6O25 with improved rate performance as negative electrode material for Li-ion batteries. Compos. B Eng. 25, 566–572.

Yi, T., Qiu, L., Mei, L., Qi, S., Cui, P., Luo, S., Zhu, Y., Xie, Y., He, Y., 2020a. Porous spherical NiO@NiMoO4@PPy nanoarchitectures as advanced electrochemical pseudocapacitor materials. Sci. Bull. 65, 546–556.

Yi, T., Wei, T., Li, Y., He, Y., Wang, Z., 2020b. Efforts on enhancing the Li-ion diffusion coefficient and electronic conductivity of titanate-based anode materials for advanced Li-ion batteries. Energy Storage Mater. 26, 165–197.

Zhang, S., Xu, K., Jow, T., 2002. A thermal stabilizer for LiPF6-based electrolytes of Li-ion cells. Electrochem. Solid-State Lett. 5, A206–A208.

Zhao, Y., Liu, M., Lv, W., He, Y., Wang, C., Yun, Q., Li, B., Kang, F., Yang, Q., 2016. Dense coating of Li4Ti5O12 and graphene mixture on the separator to produce long cycle life of lithium-sulfur battery. Nano Energy 30, 1–8.

Zheng, H., Ncube, N.M., Raju, K., Mphahlele, N., Mathe, M., 2016. The effect of Polyaniline on TiO2 nanoparticles as anode materials for Lithium Ion Batteries. SpringerPlus 5 (630).